1 # Antarctic ice-rise formation, evolution and stability

Lionel Favier,[1] Frank Pattyn,[1]

Corresponding author: L. Favier, Laboratoire de Glaciologie, Université Libre de Bruxelles, CP160/03, Av. F. D. Roosevelt 50, BE-1050 Brussels, Belgium (lionel.favier@ulb.ac.be)

[1]Laboratoire de Glaciologie, Université Libre de Bruxelles, Brussels, Belgium.

Antarctic ice rises originate from the contact between ice shelves and one of the numerous topographic highs emerging from the edge of the continental shelf. While investigations of the Raymond effect indicate their millennial-scale stability, little is known about their formation and their role in ice-shelf stability. Here, we present for the first time the simulation of an ice rise using the BISICLES model. The numerical results successfully reproduce several field observable features, such as the substantial thinning downstream of the ice rise, and the successive formation of a promontory and ice rise with stable radial ice-flow center, showing that ice rises are formed during the ice sheet deglaciation. We quantify the ice rise buttressing effect, found to be mostly transient, delaying grounding line retreat significantly but resulting in comparable steady state positions. We demonstrate that ice rises are key in controlling simulations of Antarctic deglaciation.

1. Introduction

Ice rises are locally grounded areas in floating ice shelves of the Antarctic ice sheet that can significantly reduce the flow speed of ice shelves through what is known as the buttressing effect [*Gudmundsson*, 2013]. Most Antarctic ice rises are characterized by the Raymond effect, which involves a higher effective viscosity underneath the divide compared to the flanks, due to the nonlinear nature of the flow law of ice (*Raymond* [1983]; *Conway et al.* [1999]). Analysis of the Raymond effect informs on long-term stability of ice rises. Given the large arches developed in the internal ice layers underneath the ice divide, many ice rises are characterized by a radial ice-flow center for several thousands of years (*Martin et al.* [2006]; *Drews et al.* [2015]). The temporal stability of ice rises makes them climate archives of the last millennia. Ice rises also play an active role in ice-shelf stability and their removal may lead to ice-shelf instantaneous speedup of up to 50% [*Borstad et al.*, 2013]. To date, however, studies on the transient evolution of ice rises, how they form and what determines their stability, are sparse.

Topographic highs on the continental shelf underneath ice shelves may induce the formation of either an ice rumple or an ice rise, once the ice shelf bottom is in contact with the so-called pinning point. Ice rumples are characterized by an overriding ice sheet and hence do not induce horizontal divergence of the main ice flow direction. Their formation has been previously studied numerically by *Favier et al.* [2012], who investigated how local grounding of an ice shelf has an important effect on grounding line advance: pinning of the ice shelf substantially increases buttressing, slows down the ice shelf and makes the grounding line advance until it engulfs the ice rumple that has formed on top of the pinning point.

When the contact between an ice shelf and the pinning point is lost, one expects that the subsequent loss of buttressing leads to an acceleration of the ice and subsequent retreat of the grounding line (see the verification experiment by *Favier et al.* [2012]). However, acceleration of an ice sheet due to unpinning of the ice shelf has not been clearly demonstrated so far. In the Amundsen sea sector, the eastern ice shelf of Thwaites Glacier has been accelerating since 2008 [*Mouginot et al.*, 2014]. This could be explained by a progressive unpinning of the ice shelf at its terminus [*Tinto and Bell*, 2011] or by a retreat of the grounding line caused by enhanced sub-ice shelf melting [*Mouginot et al.*, 2014]. Moreover, ungrounding of the eastern ice shelf of Thwaites Glacier seems to have little influence on the ice mass flux according to a recent model study [*Joughin et al.*, 2014].

Unlike an ice rumple, an ice rise exhibits a radial ice-flow center separate from the main ice sheet. The dynamics of an ice rise are clearly disconnected from the neighboring ice shelf which flows around the obstacle. Ice rumples and ice rises are common around the Antarctic ice sheet. For instance, they are found in the Amery ice shelf [*Fricker*, 2009], in the Ross ice shelf with the Crary and Steershead ice rises [*Fahnestock et al.*, 2000] and Roosevelt Island [*Martin et al.*, 2006], in the Larsen C ice shelf with the Bawden and Gipps ice rises [*Jansen et al.*, 2010], and in the Ronne ice shelf with the Korff and Henry ice rises surrounding the Doake ice rumples [*Johnson and Smith*, 1997]. They are also numerous along the Dronning Maud Land (DML) coast in East Antarctica and may therefore strongly affect ice sheet stability in this region. Yet, observations along the DML coast show stable ice rises and ice-rise promontories within the ice shelf, all defined by a flow center and, according to the developed Raymond effect, they have been stable features for thousands of years (*Drews et al.* [2013]; *Drews et al.* [2015]).

A prior attempt to simulate an ice rise was done by *Goldberg et al.* [2009]. The numerical experiment consisted in adding a pinning point underneath the ice shelf of a steady state ice sheet. Buttressing induced by the pinning point led to an advance of the grounding line, such as the one caused by the ice rumple in *Favier et al.* [2012], but the ice rise created was not stable and eventually swallowed by the advancing ice sheet.

Therefore, the transient formation of ice rises within an ice shelf and their supposed stability for millennia have never been simulated. Moreover, given the low spatial resolution, current ice shelf models of the Antarctic ice sheet fail to reproduce the formation and/or disintegration of ice rises, as they are initially considered grounded features within the ice shelf. The potential of ice rises to buttress ice sheets should be more investigated by proper simulations.

In order to gain an insight in the formation and evolution of ice rises, we test the hypothesis that ice rises are formed during deglaciation and subsequent grounding line retreat across the continental shelf since the Last Glacial Maximum (LGM). During that period, the East Antarctic ice sheet advanced to the continental shelf margin in some parts of East Antarctica, and the ice sheet characteristically thickened by 300-400 m near the present-day coastline at these sites [*Mackintosh et al.*, 2014]. This advance was associated with the formation of low-gradient ice streams that grounded at depths greater than 1 km below sea level on the inner continental shelf [*Mackintosh et al.*, 2014].

With a state-of-the-art ice sheet model, we simulate the deglaciation of a grounded ice sheet resting over a continental shelf-like topography across a topographic high. Grounding-line retreat is triggered by a constant rate in sea level rise over millennia. During the retreat, the topographic high gives rise to the development of an ice rise promontory and subsequently a local-flow ice rise, for which a steady state ice-sheet/shelf system is obtained. Results are compared with a simulation lacking the topographic high to inform about the effect of ice rises on ice shelf stability, buttressing and grounding-line migration rates.

2. Methodology

2.1. Experimental setup

The experimental setup is similar to other studies investigating grounding-line retreat of the Antarctic ice sheet, using a synthetic bed topography (*Schoof* [2007]; *Gudmundsson et al.* [2012]; *Gudmundsson* [2013]). In case of absence of lateral buttressing of the ice shelf (plane strain), grounding line migration occurs across retrograde bed slopes, *i.e.*, a bed slope that slopes inland, which is also known as the condition to provoke marine ice sheet instability (*Weertman* [1974]; *Schoof* [2007]; *Durand et al.* [2009]). The bedrock profile is similar to the one provided by *Schoof* [2007] and describes from the center of the ice sheet a gently lowering bedrock in the direction of the ice flow, a slight overdeepening in the coastal zone and a steep dip representing the edge of the continental shelf. This dip will also limit the maximum seaward extent of the grounding line (and the edge of the grounded ice sheet). The overdeepening facilitates grounding line migration, as in the absence of buttressing, the grounding line will not reach a steady state position during advance or retreat, as corroborated by theoretical studies (*Weertman* [1974]; *Schoof* [2007]).

For the experiments, we used two types of bed topography b and b_r, respectively, defined as:

$$\begin{aligned} b(x,y) &= b_r(x) + b_m(x,y) \\ b_r(x) &= \ 600 - 2184.8 \times A(\left(\frac{\alpha x}{750\,km}\right)^2 + \\ &\quad 1031.72 \times \left(\frac{\alpha x}{750\,km}\right)^4 - 151.72 \times \left(\frac{\alpha x}{750\,km}\right)^6) \\ b_m(x,y) &= 751 \times exp\left(\frac{-(x-650\,km)^2 - y^2}{2 \times (15\,km)^2}\right) \end{aligned} \tag{1}$$

The bed b_r (Figure 1) is a scaled version of the *Schoof* [2007] bed profile, but adapted to decrease the length of the domain and hence the computation time with the higher-order ice sheet model. In the modified bed b, a 2D Gaussian function was superimposed to b_r to add the topographic high.

Glacial Isostatic Adjustment (GIA) is not considered in our model runs, to keep the idealized setup as simple as possible. However, in reality GIA may aid in raising subglacial highs and favor pinning of the ice shelf due to mass loss during grounding line retreat.

Two types of experiments are performed with the two different bedrock setups b and b_r. They are further referred to as *iceRise* and *noRise*, respectively (Figure 1b). In both cases, a spin-up is necessary to build the initial steady state, which is obtained after 5 ka. The resulting grounding lines are then located downstream of the retrograde slope area.

The retreat of the ice sheet is triggered through a rise in sea level of 1 cm per year during 15 ka, leading to an overall rise of 150 m. For the *iceRise* experiment, the peak of the topographic high is initially at 120 m above sea level and reaches 30 m below sea level at end of the 15 ka sea level rise. For both experiments, the grounding line retreats into the retrograde slope area, passes the topographic high in the *iceRise* experiment and stabilizes on the downward sloping part of the bedrock profile (Figure 1a). The final steady states are reached after 30 ka.

2.2. Ice sheet model

We use the freely-available adaptive mesh finite-volume ice-sheet model BISICLES[1] (see *Cornford et al.* [2013] for a comprehensive overview of the model characteristics). BISICLES solves the Schoof-Hindmarsh approximation (L1L2) of the full Stokes equations on an adaptive horizontal grid produced with the Chombo adaptive mesh refinement (AMR) toolkit. The L1L2 approximation is based on the Shallow Shelf Approximation (SSA) in which the vertical shearing terms are neglected in the expression of the strain rate and stress tensors, but are included in the effective viscosity expression [*Schoof and Hindmarsh*, 2010]. While the effective viscosity calculation incorporates vertically integrated stresses, the component of mass flux due to vertical shearing is neglected because of its effect of significantly reducing the timestep. However, with respect to grounding-line migration, this approximation in combination with a sub-kilometer grid spacing across the grounding line gives results that are in accord with full Stokes modeling [*Pattyn et al.*, 2013]. Furthermore, grounding-line dynamics are better represented than in conventional SSA models or *Pollard and DeConto* [2012]-type parameterizations [*Pattyn and Durand*, 2013].

Besides the physical basis of the model, a sub-kilometric spatial resolution is a necessary condition to guarantee grounding-line migration (*Pattyn et al.* [2013]; *Pattyn and Durand*

[2013]), therefore the resolution ranges between 500 m at the grounding line and 4 km at the ice sheet divide and the calving front. Ice rheology is controlled by the Glen's flow law, and the interaction between the bed and the ice bottom surface by a Weertman-type nonlinear friction law [*Weertman*, 1957]. All model parameters are listed in Table 1.

3. Results

Since the weak topographic high is engulfed by the grounded ice sheet at the initial state, there is hardly any surface expression of the topographic effect (Figure 1b). Therefore, both initial steady states are comparable. Due to the limited influence of the topographic high, the initial grounding line is barely curved in plan view. Also the final shape of the grounding line follows a straight line.

The grounding line of the *iceRise* experiment is initially located approximately 1 km downstream of its position in the *noRise* experiment and both initial volume above flotation are quite similar within a few percent. *Durand et al.* [2011] studied the effect of a topographic high beneath a 2D grounded ice sheet on its volume above flotation and grounding line position in steady state, for different distances to the grounding line and height above the bed of the topographic high. In our simulations, this height is about 500 m above the bed and the high is located 70 km upstream of the grounding line at the initial steady state. For topographic highs with similar height and distance to the grounding line, the study by *Durand et al.* [2011] gave similar results, even though their simulation was 2D and used a linear downsloping bed towards the sea.

In our simulations, the topographic high has a more pronounced influence on the final steady state grounding line position. The non-buttressed ice shelf (not influenced by the topographic high) retreats 25 km farther inland compared to the buttressed ice shelf, which clearly demonstrates the effect of the buttressing involved by the newly established ice rise (see below).

During both experiments, the ice sheet retreats is due to the so-called Marine Ice Sheet Instability (MISI), when the grounding line enters a retrograde slope area. The MISI hypothesis was developed by *Thomas and Bentley* [1978] and *Weertman* [1974], and further verified through a boundary layer theory by *Schoof* [2007]. It has been used to verify ice sheet models under idealized situations in a series of ice-sheet model intercomparisons [*Pattyn et al.*, 2012a]. Once the grounding line retreats within the retrograde slope section, the grounding line ice thickness increases, which must be balanced by an increased flux. This, in turn, makes the grounding line retreat farther inland inducing thickness and ice flux increase. In our experiments, the buttressing induced by the ice rise is much more effective on the retreat timing than it is on steady states. This is particularly true in the comparison for the ice flux computed at the inland grounding line (Figure 2b). The maximum rate of the grounding line retreat is 150 m a^{-1} during the *noRise* experiment, which is about twice the corresponding rate simulated during the *iceRise* experiment. Moreover, as shown by Figure 2a, the non-buttressed ice sheet response occurs about 2 ka earlier. Those differences in the grounding line retreat rates and timing lead to a maximum difference of 200 km between the grounding lines after about 18 ka (Figure 2a), cause large differences in ice flux at the grounding line (Figure 2b) and consequent sea level contribution (Figure 2c).

Contrary to the *noRise* experiment where the grounding line is not influenced by lateral variations in ice flow, the grounding line in the *iceRise* experiment curves progressively around the topographic high between 15 and 19 ka (Figures 1a$_i$ and Supplementary Movie S1). This curving first elucidates an ice-rise promontory, characterized by a local peak and separated from the main ice sheet by a saddle. The local peak equally induces local ice flow with flow speeds that are several orders of magnitude lower than the flow speeds of the surrounding ice shelf (Figures 1a$_i$). During the next 500 years, the saddle area disconnects from the main grounded ice sheet and an ice rise appears. For the remaining time of the simulation, the main features of the ice rise barely change until the final steady state is reached. The final curvature of the main grounding line is straight, as it obviously is without the ice rise effect. This underscores that once the ice rise develops during grounding line retreat, it becomes a stable feature within the ice shelf.

Along flow, the surface shape of the ice rise is asymmetric (Figure 1b), the upstream slope being gentler than the downstream side. In the central flowline, the closer to the ice rise, the higher the longitudinal compression (Supplementary Movie S2), which slows down the ice shelf flow and increases the thickness upstream of the ice rise. Downstream of the ice rise, the ice flow is extensive and generates much thinner ice compared to upstream of the ice rise. Those thickness differences between the two longitudinal sides of the ice rise lead to a shift between the positions of the ice rise and the topographic high summits, the former being located about 7 km upstream of the latter (Figures 1a$_i$).

4. Discussion

Many of the features simulated here are currently observable on real ice rises and ice shelves. The ratio between ice velocities on the ice rise, in the range 0-10 m a^{-1}, and those on the neighboring ice shelf, in the range 100-1000 m a^{-1}, differs by three orders of magnitude, which compares well with the DML coast (Figure 3). Such a large ratio across the sharp transition between the ice rise bottom flanks and the ice shelf generates high strain rates and associated internal extensive stresses of hundreds of kPa (Supplementary Movie S2). This is comparable to the tensile strength of ice indicated in *Rist et al.* [1999] that would lead to the observed rifting in similar areas of ice sheets. Also observable in reality is the asymmetry in ice thickness upstream and downstream of the ice rise along the central flowline. Upstream of the ice rise, the ice is compressed and hence slows down rapidly as it gets closer to the ice rise, which induces a thickening of ice (Supplementary Movie S2). Downstream of the ice rise, the opposite is true, resulting in a much thinner ice layer, only tens of meters thick. In reality, open sea is the most common situation behind ice rises (Figure 3). However, this is not reproducible by BISICLES for the model does not account for a calving or a damage law, but such a situation can be guessed from the thin layer of ice simulated downstream of the ice rise.

Ice-rise promontories, characterized by a local ice flow and connected to the main ice sheet through a saddle area, are commonly observed along the coast of DML, as well as completely isolated ice rises (Figures 3b,c,d,e). There, the end of the last deglaciation occurred between 6 and 10 thousand years ago [*Mackintosh et al.*, 2014]. Since then the grounding line has been stable. However, as observed in other parts around Antarctica

[*Jacobs et al.*, 2011], the relatively warmer water of Circumpolar Deep Water can override the continental shelf front and increase the sub-ice shelf melting at the base of ice shelves. *Hellmer et al.* [2012] simulated a warming of 2 °C over the coming century in the cavity underneath the Filchner-Ronne ice shelf, due to a redirection of the coastal current into the Filchner trough. If such a scenario would happen at the base of ice shelves in DML, the subsequent loss of buttressing may resume the retreat of the ice sheet, which, according to our simulations, may turn promontories (such as those shown in Figure 3) rapidly into ice rises. This, however, is only valid when a retrograde slope is present upstream of the present-day grounding line. For some outlet glaciers this is the case [*Callens et al.*, 2014].

The most recent modeling attempts aimed at reconstructing the ice volume in Antarctica from the last deglaciation (*Maris et al.* [2014]; *Golledge et al.* [2014]) employ ice sheet models at relatively coarse resolutions, which questions whether they guarantee a coherent migration of the grounding line and hence the retreat of the ice sheet [*Pattyn et al.*, 2013], a problem usually circumvented by applying a large amount of basal slipperiness as is the case in these model simulations. Furthermore, not all approximations to the Stokes equations are valid for transient evolution of Stokes problems, such as grounding lines or ice rises [*Pattyn and Durand*, 2013].

Our attempt to reconstruct an ice rise from Antarctic-like conditions over the last deglaciation shows that the buttressing induced by the presence of an ice rise significantly decelerates the retreat of the ice sheet during the transient state, while initial and final steady states of both buttressed and non-buttressed experiments are found to be close. Sea level, a major driver in Antarctic deglaciation [*Deschamps et al.*, 2012], has undergone major rises, such as for instance the melt water pulse 1A during which the sea level raised by 14-18 m in about 350 years [*Deschamps et al.*, 2012]. This dramatic change must have induced large increases in ocean pressure exerted on the ice sheet margins and therefore grounding line retreat. However, the timing of the retreat, which is crucial in establishing sea-level history, may be largely delayed due to the presence of subglacial highs on the continental shelf, although final grounding line positions are less affected by their presence. Furthermore, the numerous ice-rise promontories along the DML coast, as depicted in Figure 3b, may well be transient features. This may in part explain why underneath one of these domes (the promontory shown in Figure 3d) the Raymond effect is absent (unpublished data from the analysis in *Pattyn et al.* [2012b]). The same study clearly shows that the bedrock beneath the saddle between the promontory and the continental ice sheet lies 500 m below sea level, which makes the area prone to undergo a marine ice sheet instability and a subsequent retreat of the grounding line further inland (*Pattyn et al.* [2012b]; Figure 2).

5. Conclusion

We simulated for the first time the formation and evolution of an ice rise within an ice shelf and demonstrated that such a feature is the consequence of ice sheet deglaciation and inland migration of the grounding line across the continental shelf. A number of field-observable features showed up in the modeling: (i) a very low ice shelf thickness downstream of an ice rise that explains the formation of rifts, ice-shelf breakup and open water in similar areas in Antarctica; (ii) the formation of an ice-rise promontory separated from the continental ice sheet by a saddle, which are found to be transient features; and (iii) the formation of a stable ice rise characterized by a radial ice-flow center pattern on top of the topographic high pinning the ice shelf, while most of the ice flow from the ice shelf is diverted around the ice rise. Ice rises – as simulated in these experiments – seem stable features of the ice sheet-ice shelf system, although they buttress the ice sheet considerably. The stability is corroborated from field measurements of the Raymond effect [*Drews et al.*, 2015]. Buttressing due to ice rises is not a key factor in determining the position of steady-state grounding lines, which will depend on the effectiveness of the bedrock shape in marine ice sheet conditions to stabilize on retrograde slopes (*Gudmundsson* [2013]). However, ice rises do have a major influence on grounding-line retreat rates as they slow its movement across the ice shelf. Finally, this study also highlights the need for relevant ice sheet models and the importance of grounding line resolution in order to coherently reproduce highly dynamic features related to abrupt changes in sea level rise that occurred during the last deglaciation.

Acknowledgments.

This paper forms a contribution to the Belgian Research Programme on the Antarctic (Belgian Federal Science Policy Office), Project SD/CA/06A (Constraining Ice Mass Change in Antarctica, IceCon). BISICLES development is led by D. F. Martin at Lawrence Berkeley National Laboratory, California, USA, and S. L. Cornford at the University of Bristol, UK, with financial support provided by the US Department of Energy and the UK Natural Environment Research Council. Simulations were carried out using the computational facilities of the HPC computing center at Université Libre de Bruxelles.

Notes

1. http://BISICLES.lbl.gov

References

Borstad, C. P., E. Rignot, J. Mouginot, and M. P. Schodlok (2013), Creep deformation and buttressing capacity of damaged ice shelves: theory and application to Larsen C ice shelf, *The Cryosphere*, *7*(6), 1931–1947, doi:10.5194/tc-7-1931-2013.

Callens, D., K. Matsuoka, D. Steinhage, B. Smith, E. Witrant, and F. Pattyn (2014), Transition of flow regime along a marine-terminating outlet glacier in East Antarctica, *The Cryosphere*, *8*(3), 867–875, doi:10.5194/tc-8-867-2014.

Conway, H., B. L. Hall, G. H. Denton, A. M. Gades, and E. D. Waddington (1999), Past and Future Grounding-Line Retreat of the West Antarctic Ice Sheet, *Science*, *286*(5438), 280–283, doi:10.1126/science.286.5438.280.

Cornford, S. L., D. F. Martin, D. T. Graves, D. F. Ranken, A. M. Le Brocq, R. M. Gladstone, A. J. Payne, E. G. Ng, and W. H. Lipscomb (2013), Adaptive mesh, finite volume modeling of marine ice sheets, *Journal of Computational Physics*, *232*(1), 529–549, doi:10.1016/j.jcp.2012.08.037.

Deschamps, P., N. Durand, E. Bard, B. Hamelin, G. Camoin, A. L. Thomas, G. M. Henderson, J. Okuno, and Y. Yokoyama (2012), Ice-sheet collapse and sea-level rise at the Bolling warming 14,600years ago, *Nature*, *483*(7391), 559–564, doi:10.1038/nature10902.

Drews, R., C. Martn, D. Steinhage, and O. Eisen (2013), Characterizing the glaciological conditions at Halvfarryggen ice dome, Dronning Maud Land, Antarctica, *Journal of Glaciology*, *59*(213), 9–20, doi:10.3189/2013JoG12J134.

Drews, R., K. Matsuoka, C. Martn, D. Callens, N. Bergeot, and F. Pattyn (2015), Evolution of Derwael Ice Rise in Dronning Maud Land, Antarctica, over the last millennia, *Journal of Geophysical Research: Earth Surface*, p. 2014JF003246, doi: 10.1002/2014JF003246.

Durand, G., O. Gagliardini, B. de Fleurian, T. Zwinger, and E. Le Meur (2009), Marine ice sheet dynamics: Hysteresis and neutral equilibrium, *Journal of Geophysical Research: Earth Surface*, *114*(F3), F03,009, doi:10.1029/2008JF001170.

Durand, G., O. Gagliardini, L. Favier, T. Zwinger, and E. le Meur (2011), Impact of bedrock description on modeling ice sheet dynamics, *Geophysical Research Letters*, *38*(20), L20,501, doi:10.1029/2011GL048892.

Fahnestock, M., T. Scambos, R. Bindschadler, and G. Kvaran (2000), A millennium of variable ice flow recorded by the Ross Ice Shelf, Antarctica, *Journal of Glaciology*, *46*(155), 652–664, doi:10.3189/172756500781832693.

Favier, L., O. Gagliardini, G. Durand, and T. Zwinger (2012), A three-dimensional full Stokes model of the grounding line dynamics: effect of a pinning point beneath the ice shelf, *The Cryosphere*, *6*(1), 101–112, doi:10.5194/tc-6-101-2012.

Fricker (2009), Mapping the grounding zone of the Amery Ice Shelf, East Antarctica using InSAR, MODIS and ICESat, *Antarctic Science*, *21*, 515–532, doi: 10.1017/s095410200999023x.

Goldberg, D., D. M. Holland, and C. Schoof (2009), Grounding line movement and ice shelf buttressing in marine ice sheets, *Journal of Geophysical Research: Earth Surface*, *114* (F4), F04,026, doi:10.1029/2008JF001227.

Golledge, N. R., L. Menviel, L. Carter, C. J. Fogwill, M. H. England, G. Cortese, and R. H. Levy (2014), Antarctic contribution to meltwater pulse 1a from reduced Southern Ocean overturning, *Nature Communications*, *5*, doi:10.1038/ncomms6107.

Gudmundsson, G. H. (2013), Ice-shelf buttressing and the stability of marine ice sheets, *The Cryosphere*, *7* (2), 647–655, doi:10.5194/tc-7-647-2013.

Gudmundsson, G. H., J. Krug, G. Durand, L. Favier, and O. Gagliardini (2012), The stability of grounding lines on retrograde slopes, *The Cryosphere*, *6* (6), 1497–1505, doi:10.5194/tc-6-1497-2012.

Hellmer, H. H., F. Kauker, R. Timmermann, J. Determann, and J. Rae (2012), Twenty-first-century warming of a large Antarctic ice-shelf cavity by a redirected coastal current, *Nature*, *485* (7397), 225–228, doi:10.1038/nature11064.

Jacobs, S. S., A. Jenkins, C. F. Giulivi, and P. Dutrieux (2011), Stronger ocean circulation and increased melting under Pine Island Glacier ice shelf, *Nature Geoscience*, *4* (8), 519–523, doi:10.1038/ngeo1188.

Jansen, D., B. Kulessa, P. Sammonds, A. Luckman, E. King, and N. Glasser (2010), Present stability of the Larsen C ice shelf, Antarctic Peninsula, *Journal of Glaciology*, *56* (198), 593–600, doi:10.3189/002214310793146223.

Johnson, M., and A. Smith (1997), Seabed topography under the southern and western Ronne Ice Shelf, derived from seismic surveys, *Antarctic Science*, *9* (02), 201–208, doi:

10.1017/S0954102097000254.

Joughin, I., B. E. Smith, and B. Medley (2014), Marine Ice Sheet Collapse Potentially Under Way for the Thwaites Glacier Basin, West Antarctica, *Science*, *344*(6185), 735–738, doi:10.1126/science.1249055.

Mackintosh, A. N., E. Verleyen, P. E. O'Brien, D. A. White, R. S. Jones, R. McKay, R. Dunbar, D. B. Gore, D. Fink, A. L. Post, H. Miura, A. Leventer, I. Goodwin, D. A. Hodgson, K. Lilly, X. Crosta, N. R. Golledge, B. Wagner, S. Berg, T. van Ommen, D. Zwartz, S. J. Roberts, W. Vyverman, and G. Masse (2014), Retreat history of the East Antarctic Ice Sheet since the Last Glacial Maximum, *Quaternary Science Reviews*, *100*, 10–30, doi:10.1016/j.quascirev.2013.07.024.

Maris, M. N. A., B. de Boer, S. R. M. Ligtenberg, M. Crucifix, W. J. van de Berg, and J. Oerlemans (2014), Modelling the evolution of the Antarctic ice sheet since the last interglacial, *The Cryosphere*, *8*(4), 1347–1360, doi:10.5194/tc-8-1347-2014.

Martin, C., R. C. A. Hindmarsh, and F. J. Navarro (2006), Dating ice flow change near the flow divide at Roosevelt Island, Antarctica, by using a thermomechanical model to predict radar stratigraphy, *Journal of Geophysical Research: Earth Surface*, *111*(F1), F01,011, doi:10.1029/2005JF000326.

Mouginot, J., E. Rignot, and B. Scheuchl (2014), Sustained increase in ice discharge from the Amundsen Sea Embayment, West Antarctica, from 1973 to 2013, *Geophysical Research Letters*, *41*(5), 1576–1584, doi:10.1002/2013GL059069.

Pattyn, F., and G. Durand (2013), Why marine ice sheet model predictions may diverge in estimating future sea level rise, *Geophysical Research Letters*, *40*(16), 4316–4320, doi:10.1002/grl.50824.

Pattyn, F., C. Schoof, L. Perichon, R. C. A. Hindmarsh, E. Bueler, B. de Fleurian, G. Durand, O. Gagliardini, R. Gladstone, D. Goldberg, G. H. Gudmundsson, P. Huybrechts, V. Lee, F. M. Nick, A. J. Payne, D. Pollard, O. Rybak, F. Saito, and A. Vieli (2012a), Results of the Marine Ice Sheet Model Intercomparison Project, MISMIP, *The Cryosphere*, *6*(3), 573–588, doi:10.5194/tc-6-573-2012.

Pattyn, F., K. Matsuoka, D. Callens, H. Conway, M. Depoorter, D. Docquier, B. Hubbard, D. Samyn, and J. L. Tison (2012b), Melting and refreezing beneath Roi Baudouin Ice Shelf (East Antarctica) inferred from radar, GPS, and ice core data, *Journal of Geophysical Research: Earth Surface*, *117*(F4), F04,008, doi:10.1029/2011JF002154.

Pattyn, F., L. Perichon, G. Durand, L. Favier, O. Gagliardini, R. C. Hindmarsh, T. Zwinger, T. Albrecht, S. Cornford, D. Docquier, J. J. Frst, D. Goldberg, G. H. Gudmundsson, A. Humbert, M. Htten, P. Huybrechts, G. Jouvet, T. Kleiner, E. Larour, D. Martin, M. Morlighem, A. J. Payne, D. Pollard, M. Rckamp, O. Rybak, H. Seroussi, M. Thoma, and N. Wilkens (2013), Grounding-line migration in plan-view marine ice-sheet models: results of the ice2sea MISMIP3d intercomparison, *Journal of Glaciology*, *59*(215), 410–422, doi:10.3189/2013JoG12J129.

Pollard, D., and R. M. DeConto (2012), Description of a hybrid ice sheet-shelf model, and application to Antarctica, *Geoscientific Model Development*, *5*, 1273–1295, doi:10.5194/gmd-5-1273-2012.

Raymond, C. F. (1983), Deformation in the vicinity of ice divides, *Journal of Glaciology*, *29*(103), 357–373.

Rist, M. A., P. R. Sammonds, S. a. F. Murrell, P. G. Meredith, C. S. M. Doake, H. Oerter, and K. Matsuki (1999), Experimental and theoretical fracture mechanics applied to Antarctic ice fracture and surface crevassing, *Journal of Geophysical Research: Solid Earth*, *104*(B2), 2973–2987, doi:10.1029/1998JB900026.

Schoof, C. (2007), Ice sheet grounding line dynamics: Steady states, stability, and hysteresis, *Journal of Geophysical Research: Earth Surface*, *112*(F3), F03S28, doi:10.1029/2006JF000664.

Schoof, C., and R. C. A. Hindmarsh (2010), Thin-Film Flows with Wall Slip: An Asymptotic Analysis of Higher Order Glacier Flow Models, *The Quarterly Journal of Mechanics and Applied Mathematics*, p. hbp025, doi:10.1093/qjmam/hbp025.

Thomas, R. H., and C. R. Bentley (1978), A model for Holocene retreat of the West Antarctic Ice Sheet, *Quaternary Research*, *10*(2), 150–170, doi:10.1016/0033-5894(78)90098-4.

Tinto, K. J., and R. E. Bell (2011), Progressive unpinning of Thwaites Glacier from newly identified offshore ridge: Constraints from aerogravity, *Geophysical Research Letters*, *38*(20), L20,503, doi:10.1029/2011GL049026.

Weertman, J. (1957), On the sliding of glaciers, *Journal of Glaciology*, *3*, 33–38.

Weertman, J. (1974), Stability of the junction of an ice sheet and an ice shelf, *Journal of Glaciology*, *13*, 3–11.

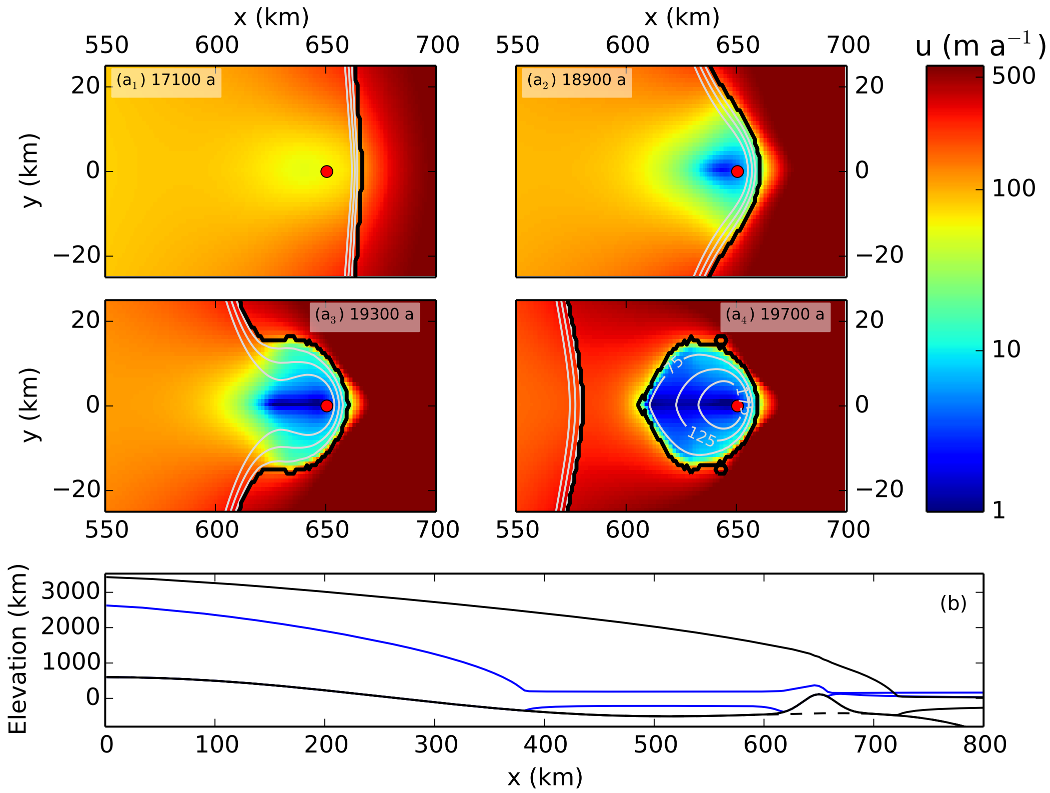

Figure 1. The four a_i figures show plan-view snapshots (elapsed time written inside the figure) of the evolution of the grounding line during the formation of the ice rise. The red dot shows the topographic high summit, the gray lines are elevation contours (shown every 50 m from 75 m to 175 m height to focus on the ice rise), and the background color displays ice velocities. The complete movie of the transient behavior is included in the Supplementary Material. (b) Elevations along the central flowline ($y = 0$). Bedrock elevation of the *iceRise* and *noRise* experiments are shown in solid and dashed black lines, respectively. The initial and final steady states of the *icerise* experiments are shown in solid black and blue lines, respectively.

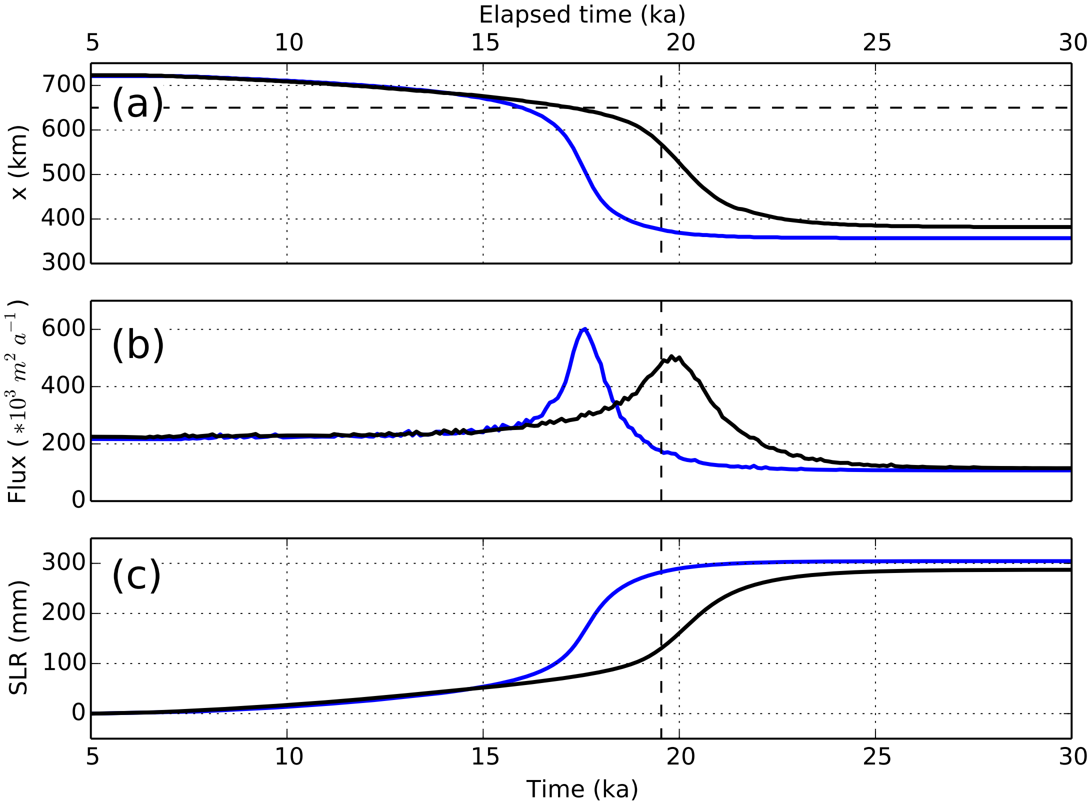

Figure 2. Retreat dynamics in between the initial and final steady states for the *iceRise* and *noRise* experiments, in solid black and blue lines, respectively. (a) Position of the most seaward grounded point and (b) ice flux at this point, both along the flowlines at both sides of the domain. (c) relative contribution to sea level rise for a 100 km wide glacier. The black horizontal (in (a) only) and vertical dashed lines represents the position of the topographic high peak and the time of creation of a separated grounded area within the ice shelf.

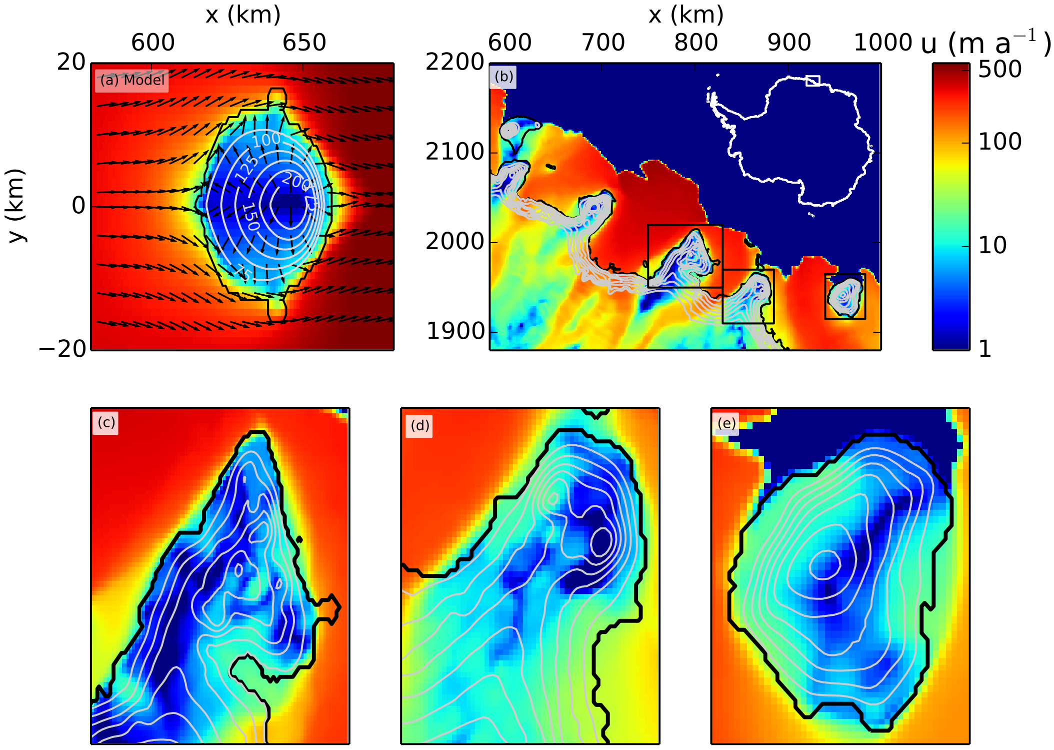

Figure 3. Ice velocity, grounding line (black line) and ice surface elevation contours (gray lines, separated by 50 m starting from 100 m high in (b,c,d,e)). (a) results of the *iceRise* experiment, (b) part of DML and (c,d,e) zooms in for different sectors each shown by a rectangle in panel (b). The Derwael ice rise is shown in (e) while two unnamed promontories are shown in (c) and (d).

Table 1. Model and bed topography parameters.

Parameter	Symbol	Value	Unit
Flow parameter	A	3.10^{-25}	Pa^{-3} s^{-1}
Seconds per year		31536000	s a^{-1}
Accumulation rate	a_s	0.3	m a^{-1}
Basal melting/accretion	a_b	0	m a^{-1}
Glen's exponent	n	3	
Bed friction parameter	C	7.624×10^6	Pa $m^{-1/3}$ $s^{1/3}$
Bed friction exponent	m	1/3	
Sea density	ρ_w	1000	kg m^{-3}
Ice density	ρ_i	900	kg m^{-3}
Gravity	g	9.8	kg m^{-3}
Domain length	L	800	km
Domain width	W	256	km
Maximum refinement		0.5	km
Bed parameter	α	1.9	
Bed parameter	A	0.75	